Journal of Water Process Engineering
Volume 38, December 2020, 101652

Anti-fouling and permeable polyvinyl chloride nanofiltration membranes embedded by hydrophilic graphene quantum dots for dye wastewater treatment

Vahid Vatanpour [a], Seyed Soroush Mousavi Khadem [b], Majid Masteri-Farahani [a], Nazanin Mosleh [a], Mohammad Reza Ganjali [b, c, d], Alireza Badiei [e], Ehsan Pourbashir [f], Amin Hamed Mashhadzadeh [b], M. Tajammal Munir [g], Ghader Mahmodi [h], Payam Zarrintaj [h], Joshua D. Ramsey [h], Seok-Jhin Kim [h], Mohammad Reza Saeb [b]

https://doi.org/10.1016/j.jwpe.2020.101652

Highlights

- Graphene quantum dots were embedded to polyvinyl chloride matrix membrane.
- GQD-embedded PVC matrix membranes reached the water flux of reached 19.1 L/m2 h.
- GQD-embedded PVC matrix membranes had bovine serum albumin rejection of more than 98%.

Abstract

In recent years, graphene has received much attention in many fields, to the extent that it has been mostly able to solve the tremendous human challenge of water scarcity. In this research, graphene quantum dots (GQDs) were used for the preparation of polyvinyl chloride (PVC) blended matrix nanofiltration membrane for removing Reactive Blue 19 dye wastewater. Improvement in anti-fouling performance was tested by filtration of bovine serum albumin (BSA) solution. The GQDs were synthesized and characterized using TEM, XRD, FTIR, UV-Vis spectrophotometer, and fluorescence emission. The surface morphology of prepared nanocomposite membranes was identified using AFM and SEM images. By embedding the optimum amount of the GQDs to the PVC matrix (1 wt%), the water flux reached 19.1 L/m^2 h, which is 56% higher than the unfilled membrane. In the case of anti-fouling properties, the flux recovery ratio was improved from 68.8 to 80.0%. All of the fabricated PVC membranes have BSA rejection of more than 98%, and Reactive Blue 19 dye rejection of more than 96%. It can be concluded that the organic anti-fouling characteristics were improved with considerable permeability enhancement without influencing membrane rejection performance.

Graphical abstract

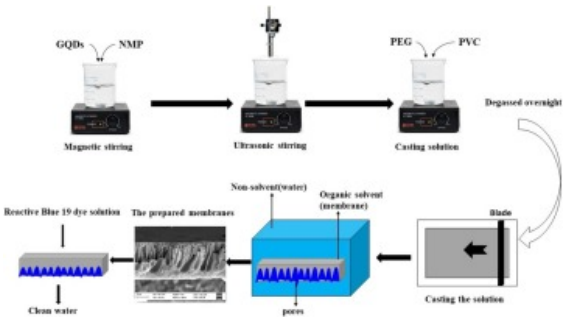

Download : Download high-res image (132KB) Download : Download full-size image

Previous Next

Keywords

Graphene quantum dots; nanocomposite membrane; anti-fouling; dye separation; environmental protection

1. Introduction

One of the most severe environmental issues is water pollution that contains various contaminants. To overcome such a problem, purification methods could be applied to provide usable water from wastewater [[1], [2], [3], [4]]. As the globe's population increases, the demand for water on limited water resources increases, hence creating a technology to recycle the wastewater is inevitable. More importantly, the filtration process, such as membranes, has attracted the attention of many researchers recently. Water scarcity causes some drastic issues, such as human and animal mortality and environmental pollution [5,6].

While resources can be optimally used and restored, the wastewater, which is composed of industrial, household, and agricultural wastewater, can be a potential resource to overcome water shortages. There are various filtration methods like coagulation, sedimentation, absorption, adsorption, and membrane processes to treat wastewater from drilling companies, agricultural runoff, and municipal sewage [[7], [8], [9], [10]].

Membranes are one of the physicochemical purification methods that can be used to filter out pollutants. Compared to the chemical treatment methods such as evaporation and thermal treatment, membrane technology is inexpensive and faster [11,12]. Incorporating various materials into the membrane matrix could improve the membrane performance depending on operating conditions. Membrane fabrication methods can be classified, such as TIPS, NIPS, VIPS, and EIPS [[13], [14], [15], [16]].

Hydrophilic nanoparticles are utilized to improve the hydrophilicity of the membranes. Physical-chemical strategies can be shown in two various forms, such as physical and chemical properties [17]. Also, the nanoparticles could improve the anti-fouling performance. Due to their high flexibility, polymer membranes play an important role in many areas such as biosensing [18], ion exchange [19], water purification [20], membrane distillation [21,22] and biomedical [23], and have achieved better performance.

Polyvinyl chloride (PVC) is one of the most popular polymers because of its benefits such as availability, inexpensive (10% PSf price), decent physicochemical, and mechanical properties such as good tensile strength. Due to the hydrophobic nature of PVC, its usage as a filtration system causes some problems, including the reduction of the permeation flux, decrement of the system efficacy, and increase in the membrane washing expenses. Hence, such a membrane should be modified in order to be used for industrial applications. [[24], [25], [26]].

Nanoparticles, because of their unique features, can be used to modify and improve the filter properties such as hydrophilicity and porosity [27]. Carbon nanotubes (CNTs) have been used in various applications due to their unique features,

mechanical strength, large aspect ratios, high surface area, distinct optical characteristics, high thermal and electrical conductivity. These properties introduce them for a broad range of utilization in the field of electronics (energy storage), biotechnology (sensors, and drug delivery) and other applications (multi-functional coatings/films) [28]. Like for instance, because of high thermal conductivity and surface area, making them useful as electrode catalyst supports in a fuel cell that is utilized in transport application, where durability is predominant [29]. Moreover, since a significant part of the human body is made up of carbon, it could be considered as a biocompatible material. CNTs are polymer containing pure carbon, which can be manipulated utilizing the extremely rich chemistry of carbon. This gives an excellent opportunity to change their structure and to maximize their solubility. More importantly, CNTs are perfect molecularly that make them free of property-damaging defects in the nanotube structure [28].

CNTs have succeeded in many challenges in the field of filtration and show an excellent anti-fouling property. Specifically, it has been used in water purification processes along with polyethersulfone (PES), polyvinylidene fluoride (PVDF), polysulfone (PSf), and PVC membranes. Using NF, UF, RO, PV mechanisms, and mixed matrix and thin films, nanocomposites structures contribute significantly to improve performance [[30], [31], [32]]. Another point is that the quantum dots (QDs) are made of nanocrystals composing a semiconductor core material [33]. QD particles have a wider bandgap and therefore require extra excitement energy for light emission at shorter wavelengths. QDs possess a wide absorption spectrum but limited fluorescent emission spectra. Such a spectrum range makes QD particularly appropriate for complex recognition, especially by employing an exciting light supplier. The QD emitting spectrum is 10-20 times brighter compared to an organic fluorophore and thousands of times more durable than traditional dyes [34]. QDs are novel nanocarbon-based materials that have been used in various fields, such as chemical assays, biosensing/bioimaging, photocatalysis, and electrocatalysis [35].

Graphene oxide quantum dots (GQDs) were selected because of their nanostructure, hydrophilic feature, and proper dispersion. As an attractive carbon-based material, GQDs have attracted significant interest in a wide range of applications because of their size, notable mechanical properties, frictionless surface, and stability [36]. One of the applications of GQDs is in the capability of targeting and imaging tumor cells simultaneously [37,38]. The broad application of GQDs was reported by Zhang et al. [39]. They researched scanning and transmission electron microscopy, and fluorescence microscopy. Zeng et al. [40] reported the covalent bonding of the GQDs onto amino-modified PVDF membranes that have anti-fouling and bactericidal better performance. There was another study on amino-functionalized GODs (aGQDs) encapsulated in thin-film nanocomposites as solvent resistance NF membranes, which were fabricated using interfacial polymerization and subsequent steps [41]. Song et al. fabricated GQDs based membranes as a chlorine resistance and anti-fouling membrane [42]. There are several nanoparticles embedded in the PVC polymer membranes in the literature. A number of these studies are summarized in Table 1.

Table 1. A number of nanoparticles embedded in the PVC polymer membranes.

Membranes	Water flux (Lm^{-2} h^{-1})	Rejection (%)	Contact angle (°)	FRR (%)	Ref.
PVC/TiO_2	316.2 (1.5 MPa)	93.7 (BSA)	49.7	84.4	[4]
EPVC/TiO_2	435 (0.2 MPa)	98 (BSA)	57.2	89.0	[43]
PVC/SiO_2	232 (0.1 MPa)	97 (BSA)	61.4	94.2	[67]
PVC/HNTs	212.2 (0.2 MPa)	93 (BSA)	77.2	92.1	[44]
PVC/ZnO	66.7 (0.04 MPa)	73.6 (COD)	46.2	87	[45]

Based on our knowledge, the effect of the addition of GQDs into PVC polymer for the fabrication of polymeric membrane has not been studied yet. In this study, our primary goal was to fabricate a novel membrane to enhance the flux and reduce the fouling of polyvinyl chloride NF membranes. The morphology and surface roughness of the membranes were investigated by scanning electron microscope (SEM) and atomic force microscopy (AFM). Anti-fouling properties were measured by BSA protein and rejection of the modified membranes by dye solution permeation that was Reactive Blue 19. This dye is one of the most common dyes used in different fiber dyeing procedures, such as dying of cotton, viscose fiber disseminated, roll dye, knot dyeing piled up, and continuous pad staining.

2. Experimental

2.1. Materials

All components were used in their analytical grade. Doubly distilled deionized water was utilized. BSA protein was bought from Sigma-Aldrich Co., USA. Citric acid monohydrate (CA), sodium hydroxide (NaOH), and glucose were purchased from Merck (Darmstadt, Germany). Suspension PVC (SPVC) was obtained from Arvand Petrochemical Co., Iran. N-methyl-2-pyrrolidone (NMP) and polyethylene glycol (PEG, MW=4000 g/mole) were received from Merck Co., Germany.

2.2. Synthesis of graphene quantum dots

Based on our previous work, CA-derived GQDs were manufactured using pyrolyzing citric acid [[46], [47], [48]]. In preparation of GQDs, citric acid (2.0 g) was poured into a beaker, and temperature elevated to 200 °C to shift the white solid citric acid to an orangish liquid. After that, 100 mL of NaOH solution (10 mg mL^{-1}) was poured dropwise into the breaker under robust stirring. The synthesized GQDs solutions can be stored at 4 °C for 30 days.

2.3. Fabrication of PVC membranes

The membranes were prepared by phase inversion method.[20]. Various amount of GQDs nanoparticles (0.05, 0.1, 0.25, 0.5, 1, and 2 wt% related to PVC) were added to solvent (NMP). The solution was placed inside the ultrasonic bath (Sonica, 2200 EP S3, Italy) for 90 min (three steps of 30 min for preventing solution heating). The sonication was used to good dispersion of GQDs in the casting solutions [49]. Then, 2 wt% PEG as a pore former, was used and mixed for 1 hour. Lastly, 18 wt% PVC was added to the precursor and stirred for 24 h. The solution was degassed by an ultrasonic bath for 10 min, and the prepared solutions were cast on the glass surface by casting applicator with a thickness of 150 μm. The fabricated membranes were transferred inside the distilled water bath until testing them.

2.4. Characterization

Fourier transform infrared spectra (FT-IR) was performed utilizing Perkin–Elmer Spectrum RXI FT-IR spectrometer with KBr pellets. The crystalline segment of the products was recognized using X-ray diffraction measurements (Cu Kα radiation (λ=1.54 Å) on a SIEFERT XRD 3003 PTS (X'PertPro) diffractometer with $10°<2\theta<80°$). The microstructure of the GQDs was evaluated with a transmission electron microscope (TEM, Hitachi H-7650). Photoluminescence (PL) spectra were obtained on a Hitachi F-7000 spectrometer (980 nm NIR laser). The optical properties of the products were analyzed with diffuse reflectance UV-vis spectroscopy, which was done on a UV-vis spectrophotometer (UV-2600, Shimadzu) by employing $BaSO_4$ as a standard material. UV-vis absorption spectra were achieved using Shimazhu UV-2450 UV-vis spectrometer.

For emission studies, 3 mL of the synthesized GQDs solution (1 mg mL^{-1} in deionized water) was placed into a quartz cuvette, and the fluorescence spectra of GQDs solutions were read under 400 nm excitation wavelength.

The hydrophilicity of the fabricated membranes was analyzed using A Goniometer apparatus (Germany). The air-water contact angle was measured ten times for obtaining reliable data. The morphology of the prepared membranes was studied by SEM characterization test (Zeiss). The samples for the cross-sectional analysis were prepared by freezing them in liquid nitrogen. All samples were subsequently sputtered with gold. NOVA (version 1.0.26) was utilized to take AFM pictures to study the topology and roughness of the prepared membranes. A scanning area of 5 × 5 μm was applied. Mean roughness (S_a), the variation between the highest and lowest peaks (S_y), the highest peak (S_z), and root mean square of the Z data (S_q) parameters were used to discuss the results of AFM. The gravimetric technique was used to calculate the porosity (ε, %) of the prepared membranes using Eq. 1 [50].

$$\varepsilon(\%) = \frac{W_2 - W_1}{\rho \times A \times l} \times 100 \quad (1)$$

Where (W_2) is the wet weight of the membranes, (W_1) is the weight of dry membranes, (ρ) the pure water density, l is the thickness of the membranes (cm), and A is the active membrane area (cm^2).

Guerout–Elford–Ferry equation (Eq. 2) was applied to calculate the average pore diameter [51].

$$r_m = \sqrt{\frac{(2.9 - 1.75\varepsilon) \times 8\eta l Q}{\varepsilon \times A \times \Delta P}} \quad (2)$$

η (Pa.s), ΔP (kPa), and Q (m^3/s) stand for water viscosity, operating pressure, and the pure water flow rate, respectively.

The viscosity of PVC casting solutions containing different amounts of GQDs was measured using Brookfield, DVIII ultra (USA) at 25 °C.

To assess the mechanical strength of the prepared GQDs/PVC membranes, tensile strength of the membranes was analyzed by INSTRON (5566, England). The tests were conducted at a rate of 1 mm/min using 500 N load cells for the samples with size of 4 × 1 cm. The average of at least four samples was reported.

2.5. Evaluation of Membrane performance

The NF membranes' performance was evaluated by a self-designed dead-end filtration set-up [52], including 8 parallel cells connected to a compressor for providing pressure (Fig. 1). The active surface area of the membrane cell is 19.6 cm^2. The treatment process was operated at four bars. Pure water, BSA solution, and dye solution were applied to examine the performance of the prepared membranes. The permeation flux, J, was calculated as follows:

$$J = \frac{V}{A \times t} \quad (3)$$

where V (L) is the volume of the permeate, A (m^2) is the active membrane surface area, and t (h) is the permeation time.

Download : Download high-res image (882KB) Download : Download full-size image

Fig. 1. The used dead-end filtration set-up for filtration tests.

Dye and BSA rejection, R, is measured by Eq. (4):

$$R(\%) = \frac{C_i - C_f}{C_i} \times 100 \quad (4)$$

Where, C_i and C_f are the concentrations of the dye or BSA in the permeate fluid and the feed solution, respectively.

2.6. Evaluation of Anti-fouling properties

After measuring the flux of the pure water, BSA solution with a concentration of 250 mg/L and pH = 7.0 was immediately put in the stirred dead-end cell. The tested membranes were cleaned by pure water for 20 min. Then, ($J_{w,2}$), the second water flux was

evaluated. To study the fouling-resistant of the modified membranes were evaluated using the flux recovery ratio (*FRR*) using Eq. (5):

$$FRR(\%) = \left(\frac{J_{w,2}}{J_{w,1}}\right) \times 100 \quad (5)$$

To more investigate the fouling process of the membranes, the fouling resistance parameters such as, intrinsic resistance (R_m) caused by chemistry, thickness, and membrane pore size: cake resistance (R_c) made by the deposited cake layer on the membrane surface: pore resistance (R_f) caused by the pore blocking: and total filtration resistance (R_t) were calculated by the following equations [37]:

$$R_m = \left(\frac{\Delta P}{\mu J_{w,1}}\right) \times 100 \quad (6)$$

$$R_f = \left(\frac{\Delta P}{\mu J_{w,2}}\right) - R_m \quad (7)$$

$$R_c = \left(\frac{\Delta P}{\mu J_P}\right) - R_m - R_f \quad (8)$$

$$R_t = R_m + R_f + R_c \quad (9)$$

3. Results and discussion

3.1. Nanomaterials Characterization

In the present study, a facile carbonization technique was utilized for the preparation of GQDs using citric acid as a carbon source. The TEM image of achieved GQDs is illustrated in Fig. 2a. The TEM image shows that GQDs are almost monodispersed nanoparticles. Moreover, the size distribution of GQDs is also displayed in the inset of Fig. 2a, which shows the mean sizes of ~6 nm for GQDs. Furthermore, the dynamic light scattering analysis (Fig. 2b) confirmed the results of the TEM image and corresponding particle size distribution. FT-IR test was applied to investigate the functional groups on the GQDs surface and use it as proof of the citric acid conversion to GQDs (Fig. 2c). The GQDs show the typical stretching vibrations of hydroxyl and carboxyl functional groups existed in the GQDs structure (Scheme 1). In GQDs, the stretching vibrations of C-H bonds are detected at ~2970 cm^{-1}, implying that the graphitization is not completed, and some aliphatic C-H bonds are available on the edges of the synthesized GQDs. The as-prepared GQDs display bonds at 1580 and 1675 cm^{-1}, which relates to the C = C and carbonyl (C = O) groups stretching, respectively [[53], [54], [55]]. A wideband at 3415 cm^{-1} is attributed to the water hydroxyl (–OH) and carboxylic groups. These bands show that the surface of GQDs is covered by hydrophilic functional groups.

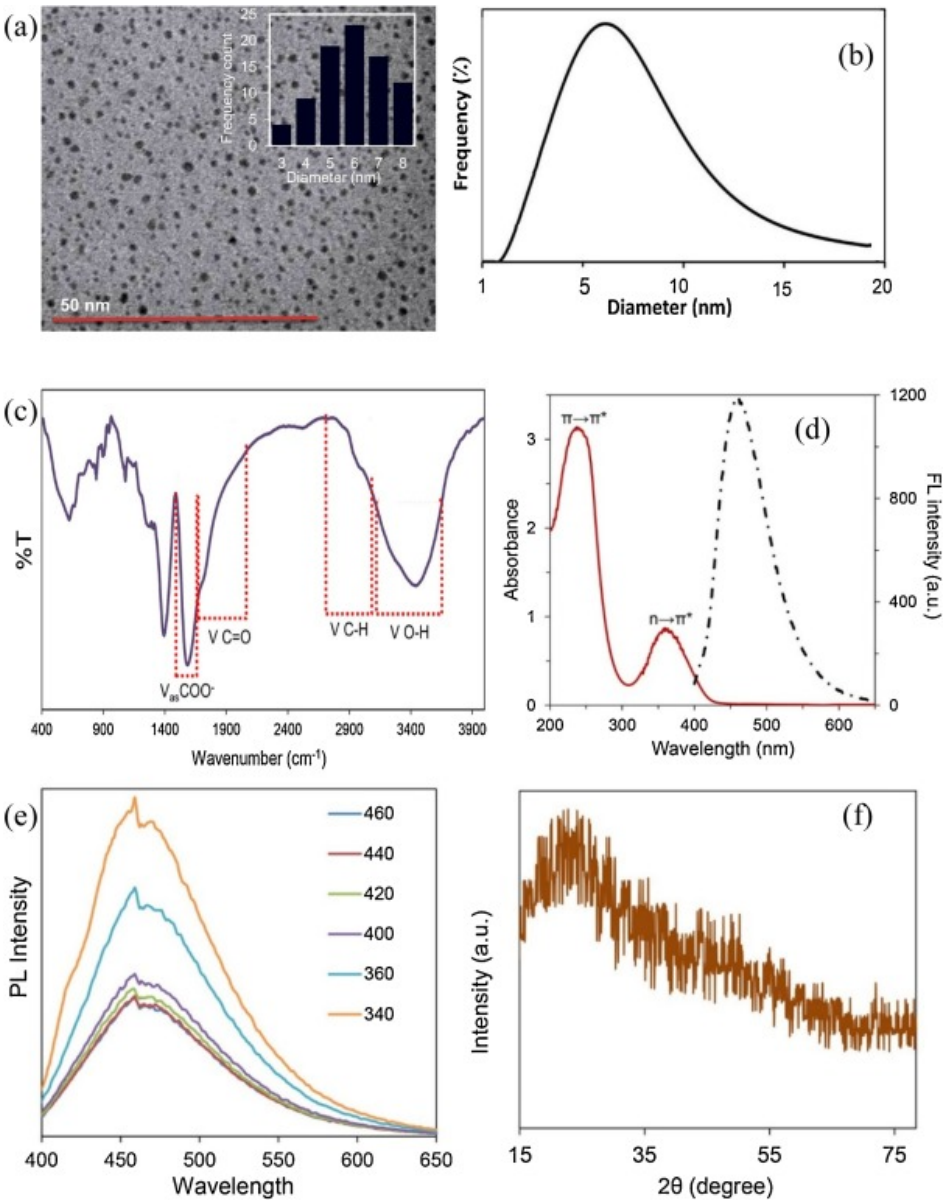

Download : Download high-res image (911KB) Download : Download full-size image

Fig. 2. (a) TEM micrograph (inset: particle size distribution), (b) DLS curve, (c) FT-IR spectrum, (d) UV-vis absorption (left axis) and fluorescence (right axis) spectra in deionized water, (e) fluorescence emission spectra in various excitation wavelengths, and (f) XRD pattern of GQDs.

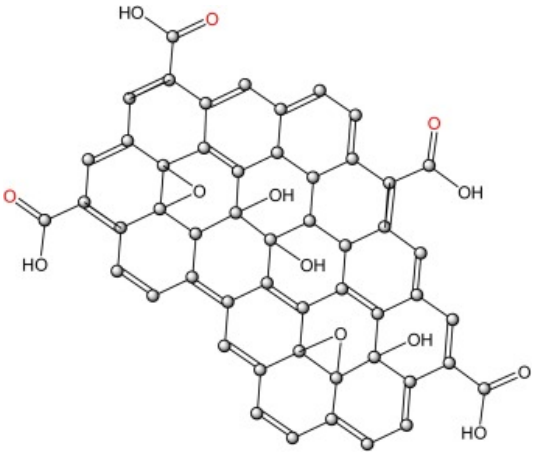

Download : Download high-res image (145KB) Download : Download full-size image

Scheme 1. Schematic representation of the GQDs structure.

The UV–Vis spectrum of GQDs (Fig. 2d) possesses two major peaks at 240 and 360 nm related to the π → π* transitions of graphitic C = C domains and n → π* transitions ascribed to the oxygen comprising functional groups, respectively [56]. Upon an excitation wavelength of 400 nm, the maximum emission of ~470 nm was acquired. As depicted in Fig. 2e, GQDs showed an excitation-independent luminescent behavior. While the source of GQDs fluorescence is a subject of recent discussion, it is totally accepted that the quantum confinement and edge effects play essential roles in such occurrence. Thus, the excitation wavelength-independence of GQDs can be related to the homogeneity in size and the surface state of those sp^2 clusters responsible for fluorescence [55].

The XRD paradigm of synthesized GQDs displays a broad diffraction peak focused at $2\theta = 25°$ (Fig. 2f), showing the relatively disordered assembling and the absence of long-range order due to the presence of several oxygen molecules including functional groups in the presented material [57].

3.2. Characterization of PVC membranes

As shown in Fig. 3, the surface morphology of the modified membranes was studied by SEM images. The surface of the pristine membrane was denser so that no obvious pores could be detected. The membrane surfaces are uniform, and there are no cracks and pinholes observed. This image demonstrates that the bare and nanocomposite membranes have no brittle construction, and the addition of GQDs has not unfavorably affected the surface of the PVC membranes. Due to black color of the used nanosheets, it visually could be seen that the membranes with higher amounts of the nanosheets has darker surface. In other words, more nanoparticles appeared on the surface due to the low dispersity and hard sonication of the GQDs nanoparticles [58,59].

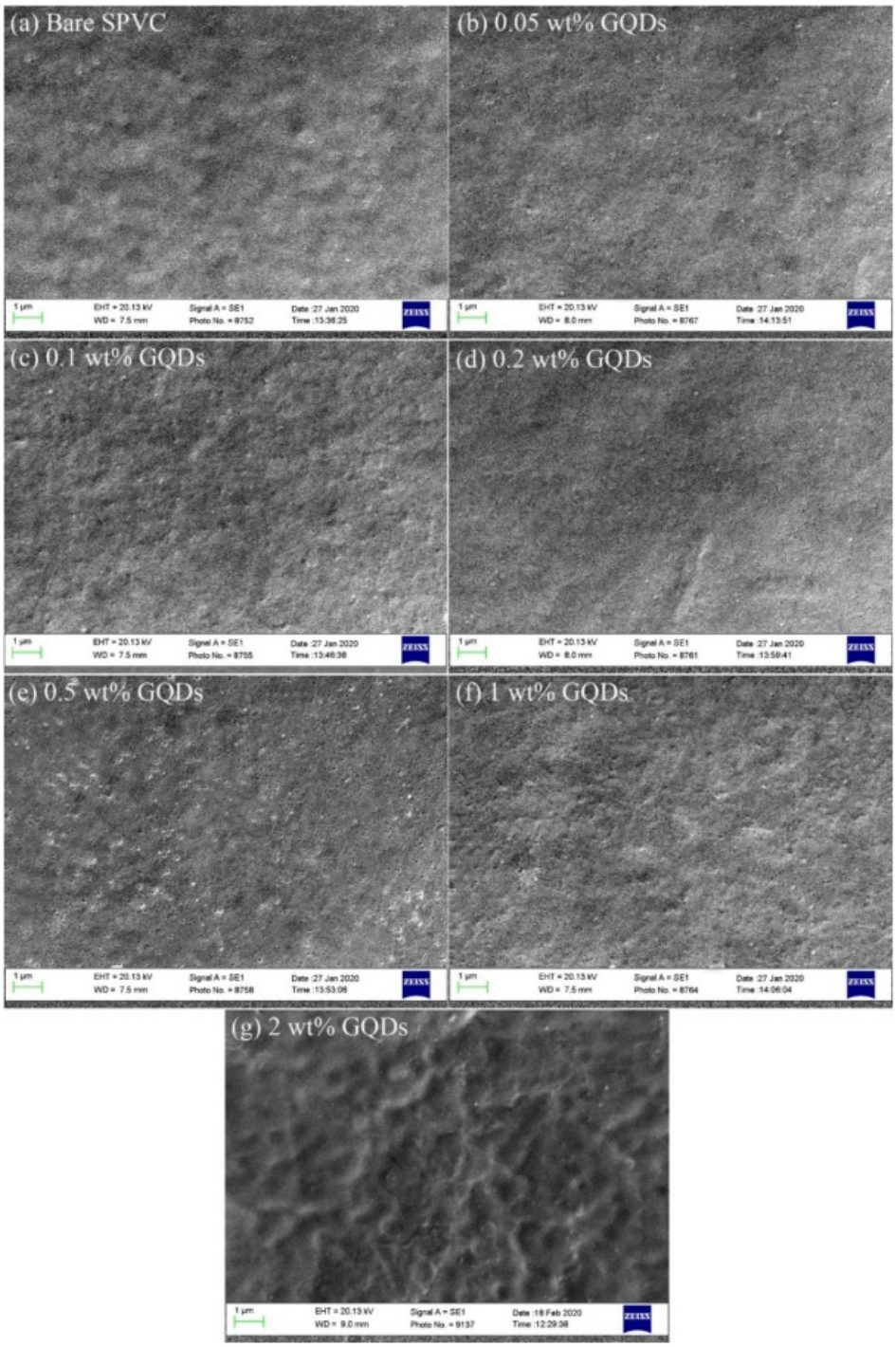

Download : Download high-res image (3MB) Download : Download full-size image

Fig. 3. Surface SEM of the PVC membranes with different amounts of GQDs.

Fig. 4 reveals the SEM views of the cross-sectional area of the membranes. It was revealed that all the synthesized membranes have an asymmetric structure that comprises a porous substrate with finger-like pores and a dense upper layer. This structure is formed due to the quick mass transmission among the solvent and the non-solvent through the non-solvent phase inversion procedure. As can be seen, by the addition of GQDs, the structure is enlarged. By comparing the cross-sectional SEM descriptions of the untouched PVC and all GQDs embedded PVC membranes, it is found that the GQDs addition to the doping solution does not alter the formation mechanism of the PVC membrane structure through the phase inversion method. By adding nanoparticles, compared with the bare PVC, it can be understood that the addition of hydrophilic GQDs

greatly accelerates the water diffusion from the coagulation bath to the polymer film (quicker rate of exchange between solvent and non-solvent), which causes the development of large finger-like or macro-voids and increases the porosity [43].

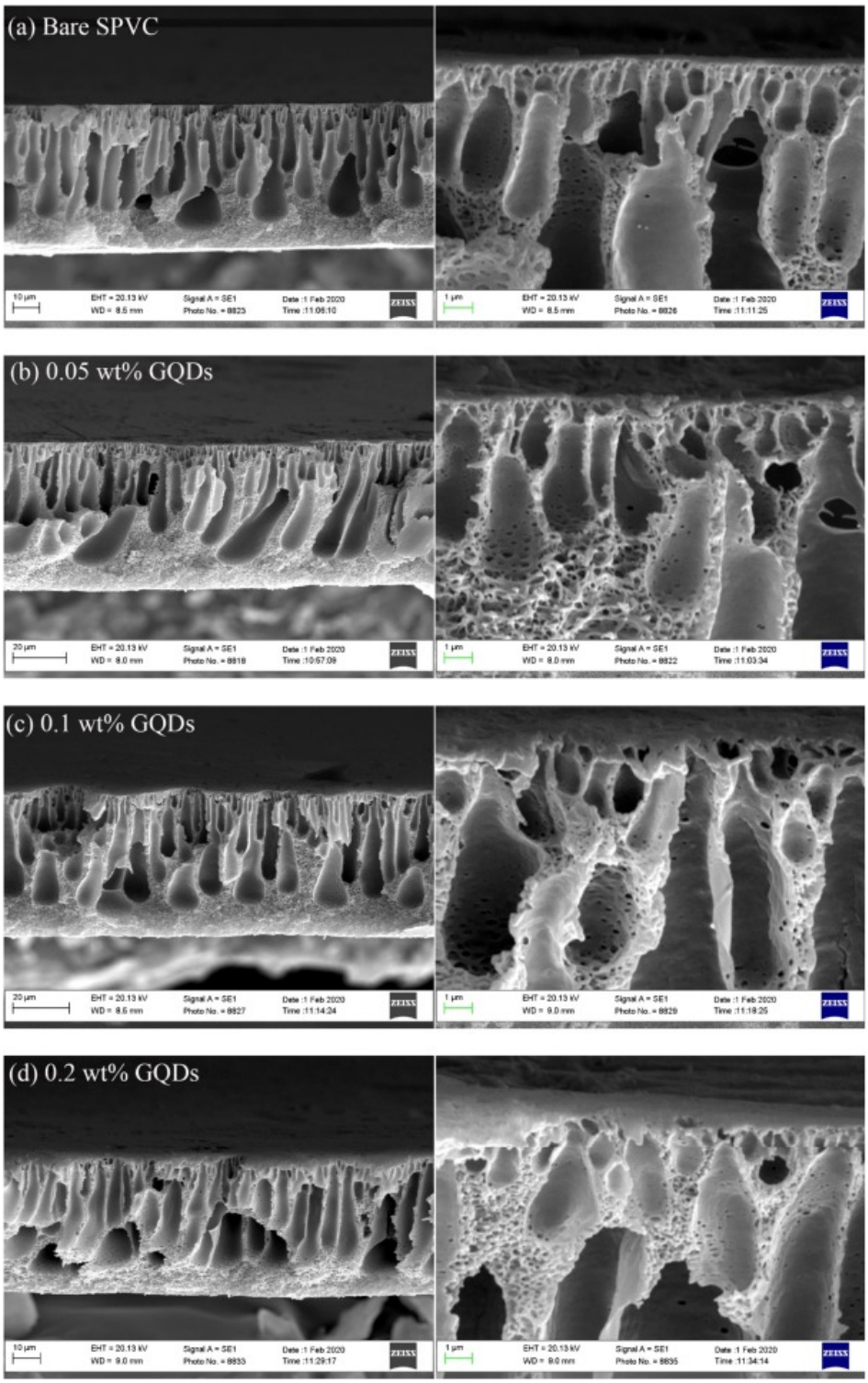

Download : Download high-res image (2MB) Download : Download full-size image

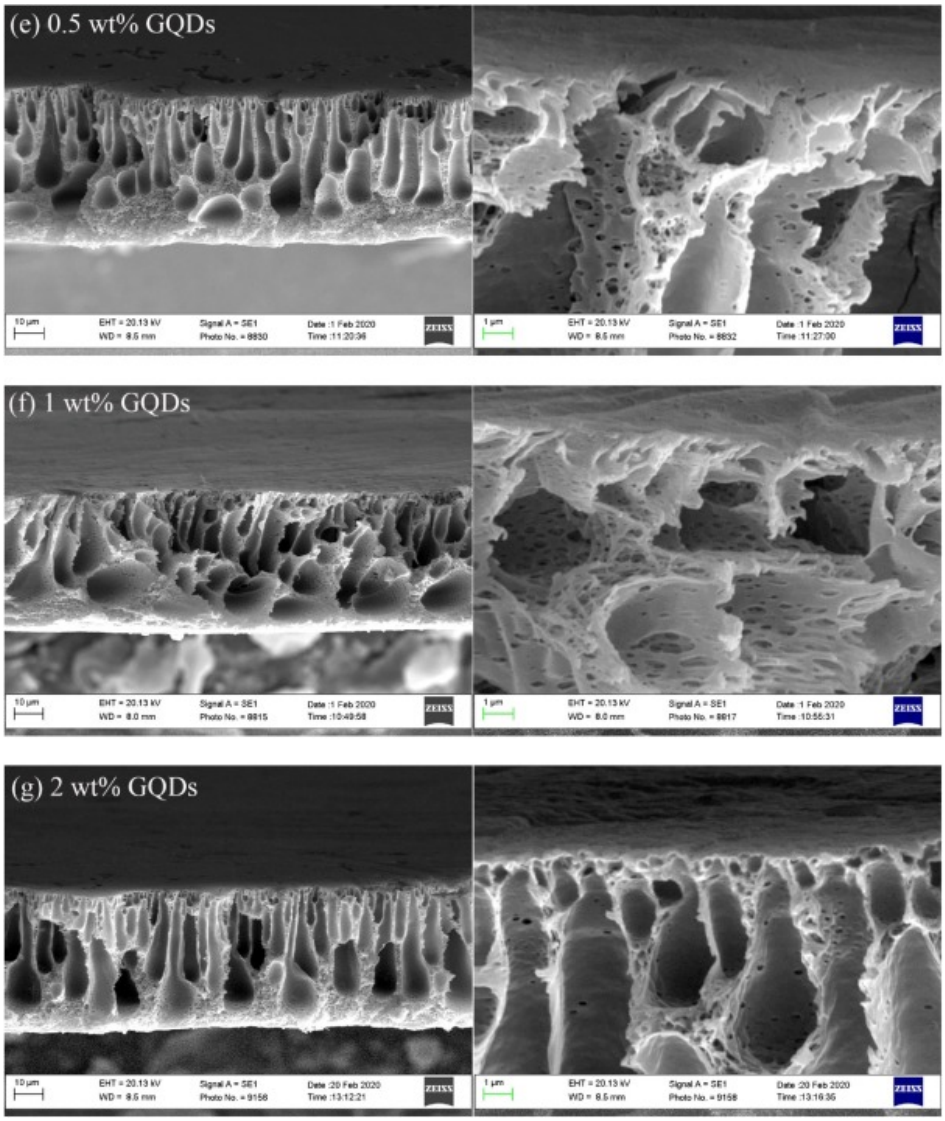

Download : Download high-res image (2MB) Download : Download full-size image

Fig. 4. Cross-sectional SEM of the GQDs/PVC membranes.

Table 2 reports porosity, average pore size, and contact angle results. In this table, which is based on the comparison of samples with nanoparticles and bare PVC, as reported in the first column, the porosity changes significantly with increasing nanoparticle percentage. The trend is the same as the mean pore size. In other words, increasing the mean pore size results in increased porosity. All samples containing GQDs have higher porosity compared to the bare sample, the highest for the 1 wt% sample. In 0.05 to 1.0 wt% membranes, an increasing trend can be observed. In this case, the porosity in the 2 wt% sample is quite similar to that in the 0.05 wt% sample. These results are quite consistent with the surface morphologies, because of the better the sample, the better the dispersity. In terms of porosity, due to the GQDs functional groups, the samples containing GQDs have better porosity. In the structure of the GQDs, there are some hydrophilic groups (approved by FTIR spectra in Fig. 2b), which could interaction with polymer chains. By growing the hydrophilicity of the dope solution with addition of the GQDs, the exchange rate of solvent/non-solvent in the phase separation process improves. Because of the rapid exchange rate of solvent/non-solvent, the overall porosity of the GQDs/PVC nanocomposite membranes was enhanced [60]. In the 2 wt% sample, the porosity is lower, probably due to the dispersity being more difficult and taking longer for sonicating. In other words, this change in membrane porosity could be analyzed by looking at the phase inversion mechanism through the membrane coagulation in non-solvent. In general, kinetics and thermodynamics are recognized as two directing parameters adjusting the formation of the phase separation membranes [45]. The viscosity results (Table 2) showed that by addition of GQDs, the viscosity

increased, which could delay the phase inversion process and prevent the instant demixing [61]. In the case of 2 wt% membrane, the viscosity effect overcome on the hydrophilicity effect and the porosity and pore size of the membrane was reduced.

Table 2. Porosity, contact angle and average pore size of the PVC membranes.

Membrane	Porosity (%)	Mean pore size (nm)	Contact angle (°)	Viscosity (cP)	Tensile Strength (MPa)
Bare SPVC	57.2 ± 2.8	2.84 ± 0.11	65.0 ± 3.4	20,146 ± 1456	13.1 ± 0.2
GQDs 0.05 wt%	66.1 ± 1.1	2.10 ± 0.19	61.9 ± 1.7	22,254 ± 1523	13.3 ± 0.3
GQDs 0.1 wt%	68.6 ± 2.1	2.51 ± 0.21	58.0 ± 3.2	24,635 ± 1635	13.5 ± 0.2
GQDs 0.2 wt%	69.4 ± 1.3	2.82 ± 0.17	57.2 ± 3.5	26,875 ± 1258	13.8 ± 0.2
GQDs 0.5 wt%	69.7 ± 3.9	3.05 ± 0.24	56.9 ± 3.1	29,874 ± 1327	14.0 ± 0.3
GQDs 1 wt%	73.0 ± 3.9	3.01 ± 0.26	55.3 ± 2.6	32,154 ± 1578	14.1 ± 0.2
GQDs 2 wt%	64.5 ± 4.5	2.89 ± 0.30	54.9 ± 2.0	35,258 ± 1367	13.9 ± 0.2

Table 2 also exhibited the viscosity results of the dope solutions by different contents of GQDs applied to fabrication of the nanocomposite membranes. With addition of the GQDs, the viscosity of the casting solutions was increased. By growing the viscosity, the phase inversion process is rheologically influenced [25,62]. The higher viscosity affects the phase inversion kinetic and overcoming the rheological property causes in diminishing the phase exchange rate during the membrane formation, forming a membrane with a lower pore size and porosity.

The same factors influence the next column reporting the mean pore sizes. That is, as the porosity rate changed, the mean pore sizes also had similar changes, which was not unexpected. By increase of the pore size, the more percent of the total volume of the membrane body will be occupied with free volume and therefore, the porosity could be improved. Given that the nanoparticles are the main cause of the porosity so that the average pore size changes and the homogeneity of the dispersity affect them, it can be seen that the size of the cavities has increased with the addition of a larger percentage of nanoparticles, with the largest size for the 1 wt% sample [41,63,64].

The third column in Table 2 shows the hydrophilicity of the samples. The contact angles of the membrane surface are recorded. According to the rule that if the contact angle is above 90 degrees, the samples are hydrophobic and have poor wetting, and if the contact angle is below 90 degrees, the samples have hydrophilic property. They were less than 90 degrees, and with adding nanoparticles, they recorded a lower contact angle than the bare sample, confirming that the samples become more hydrophilic by the addition of GQDs for water flux tests. Since the GQDs nanoparticles are inherently hydrophilic, by adding more nanoparticles, the hydrophilicity increased following [65].

To industrial application, the mechanical strength of a membrane is a significant aspect. The tensile strength of the GQDs/PVC membranes was measured to explore variations in mechanical characteristic of them, and the obtained data are presented in Table 2. The results exhibited that tensile strength of the bare SPVC membrane was 13.1 MPa and addition of GQDs enhanced tensile which could be related to the reinforcement impact of nanomaterial additive in matrix of polymer. However, at high concentration of 2 wt%, a little reduction in mechanical strength was observed, which could be related to the agglomeration of GQDs in polymer matrix [66].

Fig. 5 exhibits three- and two-dimensional AFM images of the synthesized GQDs/PVC membranes containing various percentages of the prepared nanoparticle. As a trend, the lowest average surface roughness was reported by adding 1 wt% GQDs in the membrane matrix. The surface roughness factors of the synthesized membranes including mean roughness (S_a), root mean square of the Z data (S_q), the highest peak (S_z) and the height difference between the highest peak and the lowest valley (S_y) are determined from the AFM images. Table 3 related to the roughness parameters showed that by addition of 1 wt% GQDs to the PVC casting solution, the mean roughness was reduced from 5.38 to 4.19 nm. In general, hydrophilic nanomaterials

decrease the surface roughness of polymeric membranes, which could be attributed to hydrogen bonding between functional groups (–OH, –COOH, etc.) of the nanomaterial and polymer [51]. By decreasing surface roughness, the pollutants have less chance to agglomerate in the surface valleys of the membrane. Consequently, the anti-fouling properties of the polymeric membranes are improved. Whereas, the higher surface roughness, owing to the higher surface area, causes an increase in the membrane flux [67]. The roughness amounts are slightly elevated by a further rise in GQDs to 2 wt%. The agglomeration of the GQDs on the membrane surface at a vast amount of the nanofiller could be the main reason for this increasing trend.

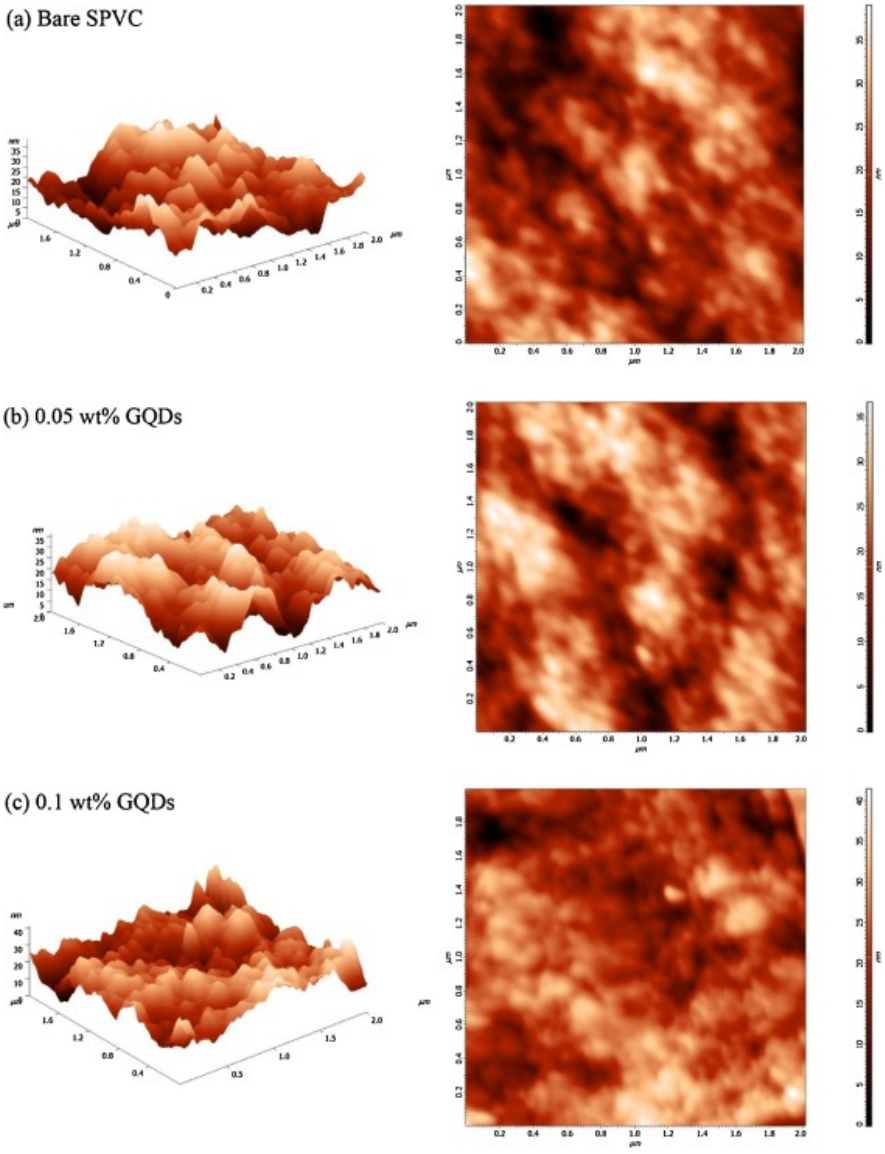

Download : Download high-res image (778KB) Download : Download full-size image

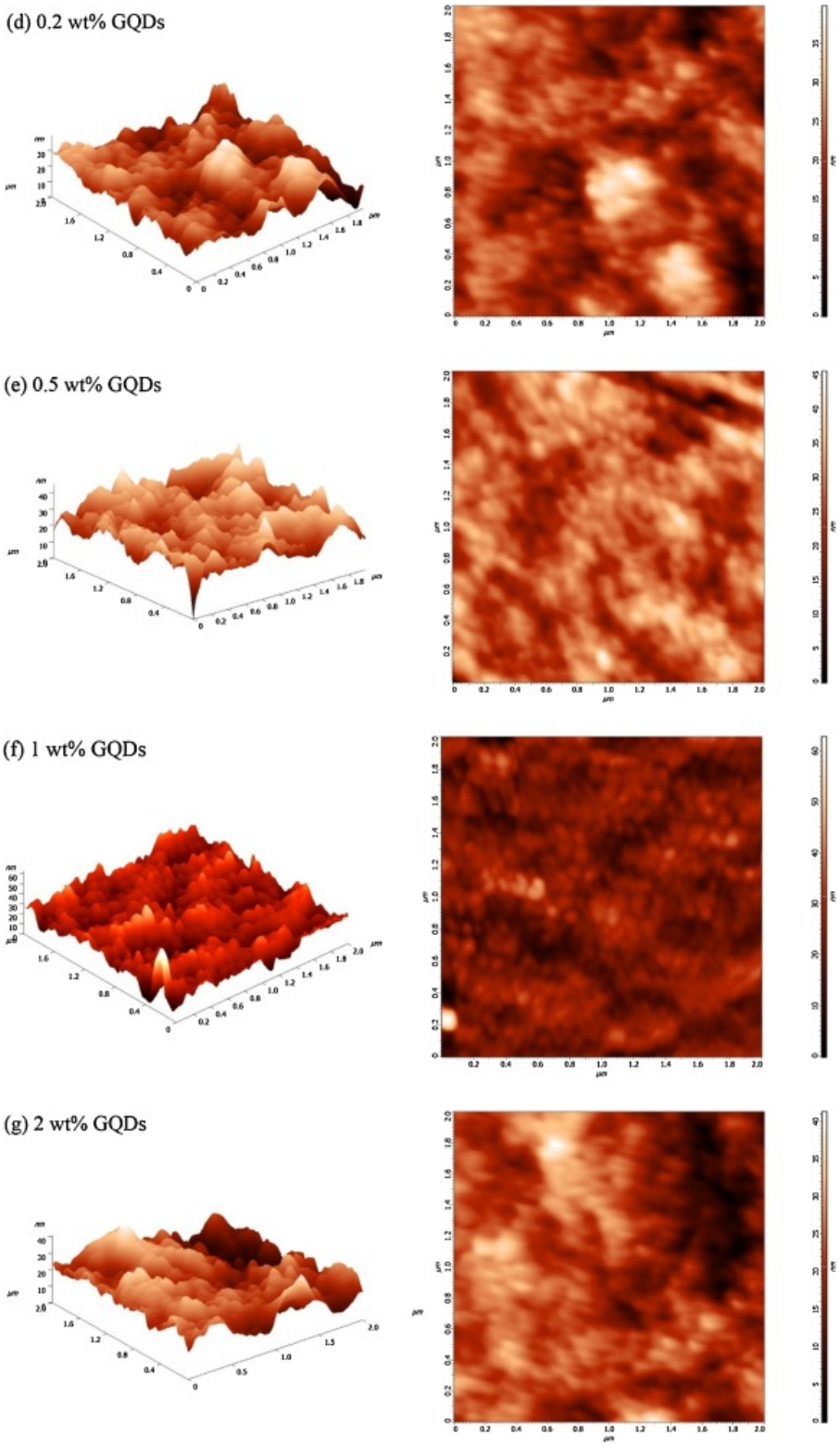

Download : Download high-res image (1MB) Download : Download full-size image

Fig. 5. AFM images of the prepared GQDs/PVC mixed matrix membranes.

Table 3. Roughness parameters of the prepared PVC membranes.

Membrane	Roughness parameters			
	S_a	S_q	S_z	S_y
Bare SPVC	5.38	6.68	19.5	38.9
0.05 wt% GQDs	5.39	6.65	18.4	36.5
0.1 wt% GQDs	4.83	6.00	20.4	41.4
0.2 wt% GQDs	4.81	6.11	20.1	39.8
0.5 wt% GQDs	4.52	5.62	23.7	45.4
1 wt% GQDs	4.19	5.50	31.4	62.6
2 wt% GQDs	5.49	6.91	20.7	41.2

3.3. Membrane filtration performance

The pure water flux from the comparison of the bare samples and GQDs-nanoparticles-containing samples is shown in Fig. 6. It can be seen that the pure water flux (PWF) ranged from 8.3 L/m^2.h for 0.05 wt% nanoparticle membrane, which was lower than 12.2 L/m^2.h for the bare membrane, to more than 19.1 L/m^2.h for 1 wt% membrane that was improved by about 40%. The increase in PWF can be ascribed to the hydrophilicity and lager membrane pore sizes. As noted, as the GQDs content of the sample increases, the mean pore radius increases. The reduction in the flux of 0.05 wt% membrane could be because of the increase of viscosity of dope solution (Table 2) by the addition of the GQDs and the decreased contribution of hydrophilicity effect. In very low concentration of the GQDs (0.05 wt%), the effect of viscosity overcomes on the hydrophilicity improvement and the pore size of the resulted membrane decreases and therefore, the flux is diminished. Although the flux rate is expected to improve by adding 2 wt% of the nanoparticles, it does not happen due to the lack of homogeneous dispersity in this amount of nanoparticles [68,69]. Overall, the flux of PVC membranes is lower than the PES membranes, and that could be due to the shorter chain in PVC or, to say the least, the less functional groups for pure water flux in this type of polymer; however, this could be resolved by the addition of hydrophilic nanoparticles [26,70].

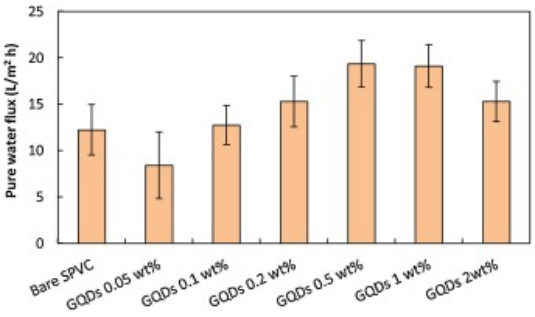

Download : Download high-res image (100KB) Download : Download full-size image

Fig. 6. Pure water flux of the GQDs/PVC membranes.

For investigating the anti-fouling properties of the synthesized GQDs/PVC membranes, after the pure water flux test, the BSA solution was filtered for 60 min. After washing the membranes for 20 min, again, the membranes test was followed by the second pure water flux filtration test. The results of all of these steps can be seen in Fig. 7. In the plot, as it is evident in the BSA test, the flux decreased over time because a layer of BSA is put on the membrane surface, reduces the amount of solution flux, and creates a resistance layer on the membrane surface, which plugs pores and fouls the membranes.

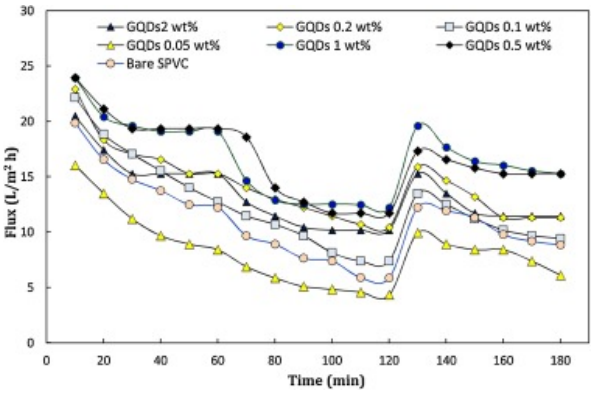

Download : Download high-res image (209KB) Download : Download full-size image

Fig. 7. Combination of pure water flux, protein flux, and second water flux for the fabricated GQDs/PVS membranes (average of at least 4 tests).

As can be seen, after washing of the membranes, the second pure water flux was very close to the first pure water flux test, especially for GQDs-containing membranes, which confirms the good performance of the fabricated membranes against the fouling.

For more details of BSA solution flux and rejection, the results of the BSA solution filtration experiments are shown in Fig. 8. It can be seen that the BSA solution flux improves with increasing GQDs percentage due to an increase in membranes porosity, mean pore size, and hydrophilicity (see Table 2). As can be seen, the 2 wt% sample has a flux drop, which is due to the agglomeration of GQDs. In all blended nanoparticle samples, the rejection percentage is approximately in the same range (more than 98%), and all rejection percentages are higher than the bare sample, which means that the percentage of nanoparticles was able to perform the removal effect well [71,72].

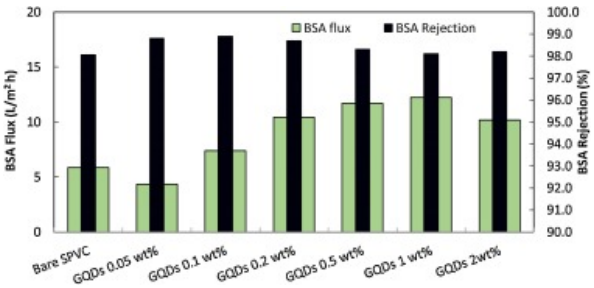

Download : Download high-res image (154KB) Download : Download full-size image

Fig. 8. BSA solution flux and rejection of the GQDs mixed matrix PVC membranes.

3.4. Anti-fouling performance

As for membrane recovery, Fig. 9 shows the flux recovery ratio of each sample after BSA filtration. In other words, the *FRR* trends showed that the flux recovery and anti-fouling properties of all GQDs-containing membranes are improved. The trend of *FRR* is similar to the first and second pure water fluxes and the BSA flux, and the highest percentage was found in 1 wt% of GQDs. In this sample, the *FRR* reaches 80%, showing good recovery operation and excellent anti-fouling characteristics. All samples with different percentages of nanoparticles had higher *FRR* than the bare sample. In the bare PVC sample, *FRR* was recorded to be 68.8%, then *FRR* was improved with the addition of nanoparticles to the membrane [73]. This anti-fouling behavior could be related to hydrophilicity improvement and decrease of surface roughness [19]. As shown in Ta

GQDs to the PVC matrix up to 1 wt%, the average surface roughness decreases, which causes less fouling of the membranes. However, in 2 wt% GQDs/PVC membrane, due to an increase of roughness parameters, the membrane fouling increased, and *FRR* was reduced.

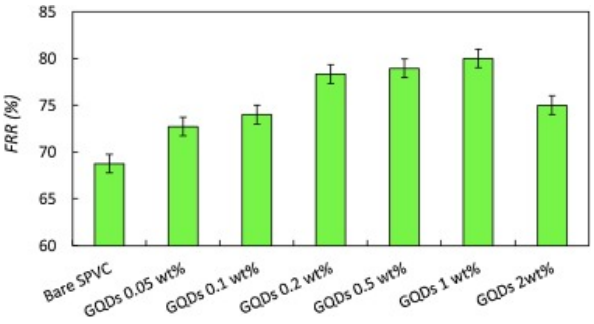

Download : Download high-res image (107KB) Download : Download full-size image

Fig. 9. The flux recovery ratio of the GQDs blended PVC membranes.

For further details on membrane clogging, all membrane resistance parameters, including pore resistance (R_p), intrinsic membrane resistance (R_m), cake resistance (R_c), and total resistance (R_t) were calculated and depicted in Fig. 10. The cake layer formed on the membrane surface, which is considered to be reversible sediment, is represented by R_c, while R_p represents the sediment resistance due to the irreversible deposition of the membrane surface and the pore attachment. Reversible sediment, unlike the irreversible type, can mostly be removed by hydraulic cleaning. Fig. 10 shows all the properties of membrane resistance. These results indicate that the overall resistance decreases with the addition of GQDs nanoparticles, and it can certainly be observed for all the mentioned resistances. The results also show that the addition of GQDs was a suitable method for reducing R_c (formed by the cake layer deposited on the membrane surface) and R_p in NF membranes [74].

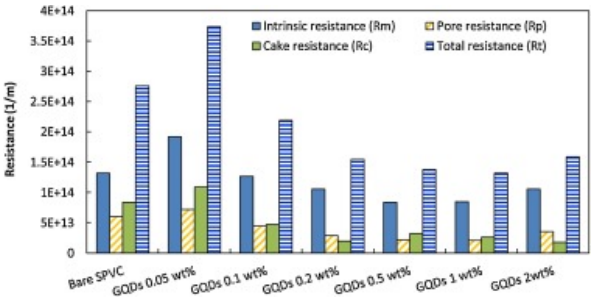

Download : Download high-res image (184KB) Download : Download full-size image

Fig. 10. Fouling parameters of the PVC nanocomposite membranes.

3.5. Dye separation

Fig. 11 shows the filtration results with color pollutants. The solution of Reactive Blue 19 dye (Fig. 11 b) with a concentration of 100 mg/L and natural pH of 5.76 was applied. The rejection percentage of all membranes was recorded to be higher than 95%, presenting excellent nanofiltration performance. The GQDs 2 wt% sample has the highest rejection percentage of 97.6%, which indicates that this sample is the most appropriate option for color removal.

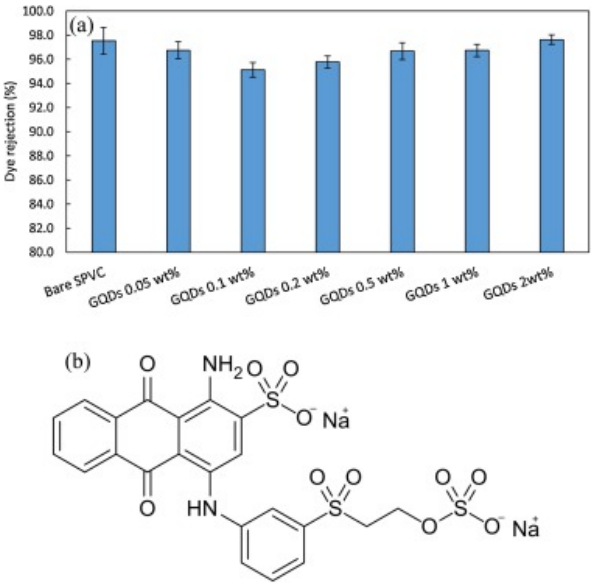

Download : Download high-res image (188KB) Download : Download full-size image

Fig. 11. (a) Dye rejection and (b) structure of Reactive Blue 19.

As shown, first, by addition of low amounts of the GQDs (0.05 and 0.1 wt%), a little reduction in the dye rejection could be seen due to increase of membrane porosity and probably presence of some big pores, which could increase the passing of the dye molecules. However, by increase of higher concentrations of the GQDs (>0.5 wt%), the functional groups of the GQDs act as a repulsion agent and the rejection was improved due to more repulsion between the functional groups of dye and embedded nanomaterials [75]. In addition, the addition of GQDs could help in enhancing the adsorption of dyes in the membrane matrix [76]. The results showed that the dye rejection of the prepared GQDs blended PVC membranes were not improved. However, in the same dye rejection ability, the anti-fouling properties and the permeability of the membranes were improved, resulting in high productivity of the membranes.

4. Conclusion

In this study, the potential of using graphene quantum dots (GQDs) as a hydrophilic nanofiller was examined for enhancing the PVC-based nanofiltration membranes. The membrane hydrophilicity was improved by increasing the GQDs amount due to the existence of functional groups on the GQDs surface, helping in improving permeability. Blending a suitable amount of the GQDs to the casting solution enlarged the porosity and mean pore diameter. The SEM images showed that the fabricated membranes possessed asymmetric shape comprising fingers like pores and a dense surface layer. The porosity, hydrophilicity, and mean pore size improvement by blending a suitable amount of GQDs resulted in the enhancement of permeability and anti-fouling property of PVC-based membranes. The pure water flux increased from 12.1 to 19.4 L/m^2 h by adding 1 wt% GQDs. The GQDs-containing membranes showed excellent performance and anti-fouling property in BSA protein solution test and dye separation test from wastewater.

Declaration of Competing Interest

The authors report no declarations of interest.

Acknowledgement

The authors would like to acknowledge Kharazmi University and the University of Tehran, Iran, for providing financial support from Kharazmi Membrane Research Core (Grant number: H/4/360). We also give special thanks to Pamela Reynolds at Oklahoma State University for editing the manuscript.

Recommended articles Citing articles (1)

References

[1] N.A. Qambrani, M.M. Rahman, S. Won, S. Shim, C. Ra
Biochar properties and eco-friendly applications for climate change mitigation, waste management, and wastewater treatment: A review
Renew. Sustain. Energy Rev., 79 (2017), pp. 255-273
Article Download PDF View Record in Scopus Google Scholar

[2] G. Mahmodi, P. Zarrintaj, A. Taghizadeh, M. Taghizadeh, S. Manouchehri, S. Dangwal, A. Ronte, M.R. Ganjali, J.D. Ramsey, S.-J. Kim, M.R. Saeb
From microporous to mesoporous mineral frameworks: An alliance between zeolite and chitosan
Carbohyd. Res., 489 (2020), Article 107930
Article Download PDF View Record in Scopus Google Scholar

[3] B. Sadeghalvad, Z. Ahali, A. Azadmehr
Modification of natural zeolite by carboxylate compounds and minerals for removal of zinc ions from wastewater: equilibrium and kinetic studies
Arab. J. Sci. Eng., 41 (2016), pp. 2501-2513
CrossRef View Record in Scopus Google Scholar

[4] A. Behboudi, Y. Jafarzadeh, R. Yegani
Preparation and characterization of TiO_2 embedded PVC ultrafiltration membranes
Chem. Engineering Res. Design, 114 (2016), pp. 96-107
Article Download PDF View Record in Scopus Google Scholar

[5] Y. Sun, Z. Chen, G. Wu, Q. Wu, F. Zhang, Z. Niu, H.-Y. Hu
Characteristics of water quality of municipal wastewater treatment plants in China: implications for resources utilization and management
J. Cleaner Prod., 131 (2016), pp. 1-9
Article Download PDF CrossRef View Record in Scopus Google Scholar

[6] T.A. Larsen, S. Hoffmann, C. Lüthi, B. Truffer, M. Maurer
Emerging solutions to the water challenges of an urbanizing world
Science, 352 (2016), pp. 928-933
CrossRef View Record in Scopus Google Scholar

[7] M.C. van Loosdrecht, P.H. Nielsen, C.M. Lopez-Vazquez, D. Brdjanovic
Experimental methods in wastewater treatment
IWA publishing (2016)
Google Scholar

[8] G. Crini, E. Lichtfouse
Advantages and disadvantages of techniques used for wastewater treatment
Environ. Chem. Lett., 17 (2019), pp. 145-155
CrossRef View Record in Scopus Google Scholar

[9] I. Sadeghi, N. Govinna, P. Cebe, A. Asatekin
Superoleophilic, mechanically strong electrospun membranes for fast and efficient gravity-driven oil/water separation
ACS Applied Polymer Materials, 1 (4) (2019), pp. 765-776
CrossRef View Record in Scopus Google Scholar

[10] B. Sadeghalvad, B.K. Moghaddam, S.A. Hamidi
Evaluation of Bassanite efficiency as an adsorbent for iron decontamination in aqueous solution

World Environmental and Water Resources Congress 2019: Groundwater, Sustainability, Hydro-Climate/Climate Change, and Environmental Engineering, American Society of Civil Engineers Reston, VA (2019), pp. 29-45
CrossRef View Record in Scopus Google Scholar

[11] M.F. Jaramillo, I. Restrepo
Wastewater reuse in agriculture: A review about its limitations and benefits
Sustainability, 9 (2017), p. 1734
View Record in Scopus Google Scholar

[12] I. Sadeghi, E.Y. Liu, H. Yi, A. Asatekin
Membranes with thin hydrogel selective layers containing viral-templated palladium nanoparticles for the catalytic reduction of Cr (VI) to Cr (III)
ACS Appl. Nano Mater., 2 (2019), pp. 5233-5244
CrossRef View Record in Scopus Google Scholar

[13] S.S. Hosseini, E. Bringas, N.R. Tan, I. Ortiz, M. Ghahramani, M.A.A. Shahmirzadi
Recent progress in development of high performance polymeric membranes and materials for metal plating wastewater treatment: A review
J. Water Proc. Eng., 9 (2016), pp. 78-110
Article Download PDF CrossRef View Record in Scopus Google Scholar

[14] W. Raza, J. Lee, N. Raza, Y. Luo, K.-H. Kim, J. Yang
Removal of phenolic compounds from industrial waste water based on membrane-based technologies
J. Ind. Eng. Chem., 71 (2019), pp. 1-18
Article Download PDF View Record in Scopus Google Scholar

[15] X. Tan, D. Rodrigue
A review on porous polymeric membrane preparation. Part I: production techniques with polysulfone and poly (vinylidene fluoride)
Polymers, 11 (2019), p. 1160
CrossRef View Record in Scopus Google Scholar

[16] F. Liu, N.A. Hashim, Y. Liu, M.R. Moghareh Abed, K. Li
Progress in the production and modification of PVDF membranes
J. Membr. Sci., 375 (2011), pp. 1-27
Article Download PDF CrossRef View Record in Scopus Google Scholar

[17] D.W. Hendricks
Water treatment unit processes: physical and chemical
CRC press (2018)
Google Scholar

[18] T. Osaki, S. Takeuchi
Artificial cell membrane systems for biosensing applications
Anal. Chem., 89 (2017), pp. 216-231
CrossRef View Record in Scopus Google Scholar

[19] J. Ran, L. Wu, Y. He, Z. Yang, Y. Wang, C. Jiang, L. Ge, E. Bakangura, T. Xu
Ion exchange membranes: New developments and applications
J. Membr. Sci., 522 (2017), pp. 267-291
Article Download PDF View Record in Scopus Google Scholar

[20] H. Rabiee, V. Vatanpour, M.H.D.A. Farahani, H. Zarrabi
Improvement in flux and anti-fouling properties of PVC ultrafiltration membranes by incorporation of zinc oxide (ZnO) nanoparticles

Sep. Purif. Technol., 156 (2015), pp. 299-310
Article Download PDF View Record in Scopus Google Scholar

[21] E. Drioli, A. Ali, F. Macedonio
Membrane distillation: Recent developments and perspectives
Desalination, 356 (2015), pp. 56-84
Article Download PDF View Record in Scopus Google Scholar

[22] I. Sadeghi, A. Asatekin
Membranes with functionalized nanopores for aromaticity-based separation of small molecules
ACS Appl. Mater. Interf., 11 (2019), pp. 12854-12862
CrossRef View Record in Scopus Google Scholar

[23] S.I. Voicu, R.M. Condruz, V. Mitran, A. Cimpean, F. Miculescu, C. Andronescu, M. Miculescu, V.K. Thakur
Sericin covalent immobilization onto cellulose acetate membrane for biomedical applications
ACS Sustain. Chem. Eng., 4 (2016), pp. 1765-1774
CrossRef View Record in Scopus Google Scholar

[24] L.-F. Fang, B.-K. Zhu, L.-P. Zhu, H. Matsuyama, S. Zhao
Structures and anti-fouling properties of polyvinyl chloride/poly (methyl methacrylate)-graft-poly (ethylene glycol) blend membranes formed in different coagulation media
J. Membr. Sci., 524 (2017), pp. 235-244
Article Download PDF View Record in Scopus Google Scholar

[25] M. Farjami, V. Vatanpour, A. Moghadassi
Effect of nanoboehmite/poly (ethylene glycol) on the performance and physiochemical attributes EPVC nanocomposite membranes in protein separation
Chem. Eng. Res. Design, 156 (2020), pp. 371-383
Article Download PDF View Record in Scopus Google Scholar

[26] P. Aryanti1, R. Yustiana1, R. Purnama, I. Wenten
"Performance and characterization of PEG400 modified PVC ultrafiltration membrane
(2015)
Google Scholar

[27] S. Xu, F. Li, B. Su, M.Z. Hu, X. Gao, C. Gao
Novel graphene quantum dots (GQDs)-incorporated thin film composite (TFC) membranes for forward osmosis (FO) desalination
Desalination, 451 (2019), pp. 219-230
Article Download PDF View Record in Scopus Google Scholar

[28] A. Venkataraman, E.V. Amadi, Y. Chen, C. Papadopoulos
Carbon nanotube assembly and integration for applications
Nanoscale research letters, 14 (1) (2019), pp. 1-47
View Record in Scopus Google Scholar

[29] B. Gao, *et al.*
Enhanced saturation lithium composition in ball-milled single-walled carbon nanotubes
Chemical Physics Letters, 327 (1-2) (2000), pp. 69-75
Article Download PDF View Record in Scopus Google Scholar

[30] M. Rashid, S.F. Ralph
Carbon nanotube membranes: synthesis, properties, and future filtration applications
Nanomaterials, 7 (5) (2017), p. 99
CrossRef View Record in Scopus Google Scholar

[31] B. Lee, *et al.*
A carbon nanotube wall membrane for water treatment
Nature communications, 6 (1) (2015), pp. 1-7
CrossRef View Record in Scopus Google Scholar

[32] M. Sianipar, S.H. Kim, F. Iskandar, I.G. Wenten
Functionalized carbon nanotube (CNT) membrane: progress and challenges
RSC advances, 7 (81) (2017), pp. 51175-51198
CrossRef View Record in Scopus Google Scholar

[33] R.S. Pawar, P.G. Upadhaya, V.B. Patravale
Quantum Dots: Novel Realm in Biomedical and Pharmaceutical Industry
Handbook of Nanomaterials for Industrial Applications, Elsevier (2018), pp. 621-637
Article Download PDF View Record in Scopus Google Scholar

[34] X. Qu, P.J. Alvarez, Q. Li
Applications of nanotechnology in water and wastewater treatment
Water research, 47 (12) (2013), pp. 3931-3946
Article Download PDF View Record in Scopus Google Scholar

[35] D.L. Zhao, T.-S. Chung
Applications of carbon quantum dots (CQDs) in membrane technologies: A review
Water Res., 147 (2018), pp. 43-49
Article Download PDF View Record in Scopus Google Scholar

[36] M. Inagaki, F. Kang, M. Toyoda, H. Konno
Chapter 3 - Graphene: Synthesis and Preparation
M. Inagaki, F. Kang, M. Toyoda, H. Konno (Eds.), Advanced Materials Science and Engineering of Carbon, Butterworth-Heinemann, Boston (2014), pp. 41-65
Article Download PDF Google Scholar

[37] Z. Su, *et al.*
Motif-Designed Peptide Nanofibers Decorated with Graphene Quantum Dots for Simultaneous Targeting and Imaging of Tumor Cells
Advanced Functional Materials, 25 (34) (2015), pp. 5472-5478
CrossRef View Record in Scopus Google Scholar

[38] X.T. Zheng, A. Ananthanarayanan, K.Q. Luo, P. Chen
Glowing graphene quantum dots and carbon dots: properties, syntheses, and biological applications
Small, 11 (14) (2015), pp. 1620-1636
CrossRef View Record in Scopus Google Scholar

[39] P. Zhang, *et al.*
Electrospinning graphene quantum dots into a nanofibrous membrane for dual-purpose fluorescent and electrochemical biosensors
Journal of Materials Chemistry B, 3 (12) (2015), pp. 2487-2496
CrossRef View Record in Scopus Google Scholar

[40] Z. Zeng, *et al.*
Graphene oxide quantum dots covalently functionalized PVDF membrane with significantly-enhanced bactericidal and antibiofouling performances
Scientific reports, 6 (2016), Article 20142
View Record in Scopus Google Scholar

[41] S. Li, C. Li, B. Su, M.Z. Hu, X. Gao, C. Gao

Amino-functionalized graphene quantum dots (aGQDs)-embedded thin film nanocomposites for solvent resistant nanofiltration (SRNF) membranes based on covalence interactions
Journal of Membrane Science, 588 (2019), Article 117212
Article Download PDF View Record in Scopus Google Scholar

[42] X. Song, Q. Zhou, T. Zhang, H. Xu, Z. Wang
Pressure-assisted preparation of graphene oxide quantum dot-incorporated reverse osmosis membranes: anti-fouling and chlorine resistance potentials
Journal of Materials Chemistry A, 4 (43) (2016), pp. 16896-16905
View Record in Scopus Google Scholar

[43] H. Rabiee, M.H.D.A. Farahani, V. Vatanpour
Preparation and characterization of emulsion poly (vinyl chloride)(EPVC)/TiO_2 nanocomposite ultrafiltration membrane
J. Membr. Sci., 472 (2014), pp. 185-193
Article Download PDF View Record in Scopus Google Scholar

[44] G. Mishra, M. Mukhopadhyay
Enhanced anti-fouling performance of halloysite nanotubes (HNTs) blended poly (vinyl chloride)(PVC/HNTs) ultrafiltration membranes: For water treatment
Journal of industrial and engineering chemistry, 63 (2018), pp. 366-379
Article Download PDF View Record in Scopus Google Scholar

[45] Q.F. Alsalhy, F.H. Al-Ani, A.E. Al-Najar, S.I. Jabuk
A study of the effect of embedding ZnO-NPs on PVC membrane performance use in actual hospital wastewater treatment by membrane bioreactor
Chemical Engineering and Processing-Process Intensification, 130 (2018), pp. 262-274
Article Download PDF View Record in Scopus Google Scholar

[46] M. Amjadi, J.L. Manzoori, T. Hallaj
Chemiluminescence of graphene quantum dots and its application to the determination of uric acid
Journal of luminescence, 153 (2014), pp. 73-78
Article Download PDF View Record in Scopus Google Scholar

[47] Y. Dong, *et al.*
Blue luminescent graphene quantum dots and graphene oxide prepared by tuning the carbonization degree of citric acid
Carbon, 50 (12) (2012), pp. 4738-4743
Article Download PDF View Record in Scopus Google Scholar

[48] T. Hallaj, M. Amjadi, J.L. Manzoori, R. Shokri
Chemiluminescence reaction of glucose-derived graphene quantum dots with hypochlorite, and its application to the determination of free chlorine
Microchimica Acta, 182 (2015), pp. 789-796
CrossRef View Record in Scopus Google Scholar

[49] M.-L. Liu, J.-L. Guo, S. Japip, T.-Z. Jia, D.-D. Shao, S. Zhang, W.-J. Li, J. Wang, X.-L. Cao, S.-P. Sun
One-step Enhancement of solvent transport, stability and photocatalytic properties of graphene oxide/polyimide membranes with multifunctional cross-linker
J. Mater. Chem. A, 7 (2019), pp. 3170-3178
CrossRef View Record in Scopus Google Scholar

[50] B. Freeman, Y. Yampolskii, I. Pinnau
Materials science of membranes for gas and vapor separation
John Wiley & Sons (2006)
Google Scholar

[51] J. Rezania, A. Shockravi, V. Vatanpour, M. Ehsani
Preparation and performance evaluation of carboxylic acid containing polyamide incorporated microporous ultrafiltration PES membranes
Polym. Adv. Technol., 30 (2019), pp. 407-416
CrossRef View Record in Scopus Google Scholar

[52] V. Vatanpour, S.S. Madaeni, R. Moradian, S. Zinadini, B. Astinchap
Fabrication and characterization of novel anti-fouling nanofiltration membrane prepared from oxidized multiwalled carbon nanotube/polyethersulfone nanocomposite
J. Membr. Sci., 375 (2011), pp. 284-294
Article Download PDF View Record in Scopus Google Scholar

[53] W. Zhang, *et al.*
Graphenol defects induced blue emission enhancement in chemically reduced graphene quantum dots
Phys. Chem. Chem. Phys., 17 (2015), pp. 22361-22366
CrossRef View Record in Scopus Google Scholar

[54] M. Masteri-Farahani, S. Mashhadi-Ramezani, N. Mosleh
Molecularly imprinted polymer containing fluorescent graphene quantum dots as a new fluorescent nanosensor for detection of methamphetamine, Spectrochimica Acta Part A: Mol
Biomol. Spectr., 229 (2020), Article 118021
Article Download PDF View Record in Scopus Google Scholar

[55] A. Dutta Chowdhury, R.-a. Doong
Highly sensitive and selective detection of nanomolar ferric ions using dopamine functionalized graphene quantum dots
ACS Appl. Mater. Interf., 8 (2016), pp. 21002-21010
CrossRef View Record in Scopus Google Scholar

[56] M. Masteri-Farahani, N. Mosleh
Functionalization of graphene quantum dots with antimorphine: Design of selective nanosensor for detection of morphine
Mater. Lett., 241 (2019), pp. 206-209
Article Download PDF View Record in Scopus Google Scholar

[57] Z. Wang, Z. Fan
Cu^{2+} modulated nitrogen-doped grapheme quantum dots as a turn-off/on fluorescence sensor for the selective detection of histidine in biological fluid, Spectrochimica
Acta Part A: Mol. Biomol. Spectr., 189 (2018), pp. 195-201
Article Download PDF View Record in Scopus Google Scholar

[58] R. Bi, *et al.*
Graphene quantum dots engineered nanofiltration membrane for ultrafast molecular separation
Journal of membrane science, 572 (2019), pp. 504-511
Article Download PDF View Record in Scopus Google Scholar

[59] G. Zhao, R. Hu, J. Li, H. Zhu
Graphene oxide quantum dots embedded polysulfone membranes with enhanced hydrophilicity, permeability and anti-fouling performance
Sci. China Mater., 62 (2019), pp. 1177-1187
CrossRef View Record in Scopus Google Scholar

[60] M.H.D.A. Farahani, H. Rabiee, V. Vatanpour
Comparing the effect of incorporation of various nanoparticulate on the performance and antifouling properties of polyethersulfone nanocomposite membranes
J. Water Proc. Eng., 27 (2019), pp. 47-57

Article Download PDF View Record in Scopus Google Scholar

[61] T.D. Kusworo, N. Ariyanti, D.P. Utomo
Effect of nano-TiO_2 loading in polysulfone membranes on the removal of pollutant following natural-rubber wastewater treatment
J. Water Proc. Eng., 35 (2020), Article 101190
Article Download PDF View Record in Scopus Google Scholar

[62] K.A. Gebru, C. Das
Effects of solubility parameter differences among PEG, PVP and CA on the preparation of ultrafiltration membranes: impacts of solvents and additives on morphology, permeability and fouling performances
Chinese J. Chem. Eng., 25 (2017), pp. 911-923
Article Download PDF View Record in Scopus Google Scholar

[63] L. Ghalamchi, S. Aber, V. Vatanpour, M. Kian
Comparison of NLDH and g-C3N4 nanoplates and formative Ag_3PO_4 nanoparticles in PES microfiltration membrane fouling: Applications in MBR
Chem. Eng. Res. Design, 147 (2019), pp. 443-457
Article Download PDF View Record in Scopus Google Scholar

[64] M. Safarpour, V. Vatanpour, A. Khataee
Preparation and characterization of graphene oxide/TiO2 blended PES nanofiltration membrane with improved anti-fouling and separation performance
Desalination, 393 (2016), pp. 65-78
Article Download PDF View Record in Scopus Google Scholar

[65] A. Colburn, N. Wanninayake, D. Kim, D. Bhattacharyya
Cellulose-graphene quantum dot composite membranes using ionic liquid
Journal of membrane science, 556 (2018), pp. 293-302
Article Download PDF View Record in Scopus Google Scholar

[66] A. Behboudi, Y. Jafarzadeh, R. Yegani
Enhancement of antifouling and antibacterial properties of PVC hollow fiber ultrafiltration membranes using pristine and modified silver nanoparticles
J. Environ. Chem. Eng., 6 (2018), pp. 1764-1773
Article Download PDF View Record in Scopus Google Scholar

[67] S. Li, *et al.*
Graphene quantum dots-doped thin film nanocomposite polyimide membranes with enhanced solvent resistance for solvent-resistant nanofiltration
ACS Appl. Mater. Interf., 11 (2019), pp. 6527-6540
CrossRef Google Scholar

[68] A. Behboudi, Y. Jafarzadeh, R. Yegani
Polyvinyl chloride/polycarbonate blend ultrafiltration membranes for water treatment
J. Membr. Sci., 534 (2017), pp. 18-24
Article Download PDF View Record in Scopus Google Scholar

[69] Z. Yu, X. Liu, F. Zhao, X. Liang, Y. Tian
Fabrication of a low-cost nano-SiO_2/PVC composite ultrafiltration membrane and its anti-fouling performance
J. Appl. Polym. Sci., 132 (2015), p. 41267
View Record in Scopus Google Scholar

[70] G. Mahmodi, S. Dangwal, P. Zarrintaj, M. Zhu, Y. Mao, D.N. Mcllroy, M.R. Saeb, V. Vatanpour, J.D. Ramsey, S.-J. Kim
NaA zeolite-coated meshes with tunable hydrophilicity for oil-water separation

Sep. Purif. Technol., 240 (2020), Article 116630
Article Download PDF View Record in Scopus Google Scholar

[71] D. Ghazanfari, D. Bastani, S.A. Mousavi
Preparation and characterization of poly (vinyl chloride)(PVC) based membrane for wastewater treatment
J. Water Proc. Eng., 16 (2017), pp. 98-107
Article Download PDF View Record in Scopus Google Scholar

[72] Y.-F. Mi, F.-Y. Zhao, Y.-S. Guo, X.-D. Weng, C.-C. Ye, Q.-F. An
Constructing zwitterionic surface of nanofiltration membrane for high flux and anti-fouling performance
J. Membr. Sci., 541 (2017), pp. 29-38
Article Download PDF View Record in Scopus Google Scholar

[73] A. Jalali, A. Shockravi, V. Vatanpour, M. Hajibeygi
Preparation and characterization of novel microporous ultrafiltration PES membranes using synthesized hydrophilic polysulfide-amide copolymer as an additive in the casting solution
Micropor. Mesopor. Mater., 228 (2016), pp. 1-13
Article Download PDF View Record in Scopus Google Scholar

[74] J.Z. Hamad, R. Dua, N. Kurniasari, M.D. Kennedy, P. Wang, G.L. Amy
Irreversible membrane fouling abatement through pre-deposited layer of hierarchical porous carbons
Water Res., 65 (2014), pp. 245-256
Article Download PDF View Record in Scopus Google Scholar

[75] D.-D. Shao, W.-J. Yang, H.-F. Xiao, Z.-Y. Wang, C. Zhou, X.-L. Cao, S.-P. Sun
Self-Cleaning Nanofiltration Membranes by Coordinated Regulation of Carbon Quantum Dots and Polydopamine
ACS Appl. Mater. Interf., 12 (2020), pp. 580-590
CrossRef View Record in Scopus Google Scholar

[76] M. la Luz-Asunción, E.E. Pérez-Ramírez, A.L. Martínez-Hernández, P.E. García-Casillas, J.G. Luna-Bárcenas, C. Velasco-Santos
Adsorption and kinetic study of Reactive Red 2 dye onto graphene oxides and graphene quantum dots
Diamond Rel. Mater., 109 (2020), Article 108002
Google Scholar

View Abstract

Published by Elsevier Ltd.